Journal of Power Sources 195 (2010) 5768–5774

Contents lists available at ScienceDirect

Journal of Power Sources

journal homepage: www.elsevier.com/locate/jpowsour

Long-term cycling studies on 4 V-cathode, lithium vanadium fluorophosphate

M.V. Reddy, G.V. Subba Rao, B.V.R. Chowdari*

Department of Physics, National University of Singapore, Singapore 117542, Singapore

ARTICLE INFO

Article history:
Received 8 January 2010
Received in revised form 17 February 2010
Accepted 1 March 2010
Available online 15 March 2010

Keywords:
Lithium vanadium fluorophosphate
Cathode
Lithium-ion batteries
Carbothermal reduction
Impedance spectroscopy

ABSTRACT

Lithium vanadium fluorophosphate, $LiVPO_4F$ is prepared by two-step carbothermal reduction method and characterized by X-ray diffraction, X-ray photoelectron spectroscopy (XPS), scanning electron microscopy (SEM), density and surface area. Its cathodic behaviour is examined by galvanostatic charge–discharge cycling up to 1260 cycles, cyclic voltammetry (CV) and impedance spectra using Li-metal as the counter and reference electrode. When cycled between 3.0 and 4.5 V at 15 mA g^{-1} (0.12*C*), a reversible and stable capacity of 130 (±3) mAh g^{-1} is observed in the range 20–200 cycles. Slow capacity fading occurs between 200 and 360 cycles. When cycled at the 0.92*C* rate (1*C* = 130 mA g^{-1}), a reversible and stable capacity of 122 (±3) mAh g^{-1} is obtained at 200–800 cycles. The capacity degrades slowly over 800–1260 cycles and the total loss is ~14%. Coulombic efficiency increases to 96–98% after the first 10–15 cycles. The CV data show that the charge–discharge process, a two-phase reaction, occurs between 4.2 and 4.5 V, in agreement with literature data. Impedance spectra, up to 90 cycles are fitted to an equivalent circuit and the variation of impedance parameters is interpreted.

1. Introduction

In 2003, Barker et al. [1] reported a new and novel 4 V-cathode material, namely, lithium vanadium fluorophosphate, $LiVPO_4F$, as an alternative to the commonly used $LiCoO_2$ in first-generation lithium-ion batteries (LIBs). It has a theoretical capacity of 156 mAh g^{-1} and operates using the redox couple $V^{3+/4+}$ during charge–discharge cycling via a two-phase reaction. Subsequent studies by Barker et al. [2–7], Li et al. [8], Zhou et al. [9] and Zhong et al. [10] have shown the following interesting properties: (i) the average lithium-de-intercalation–intercalation voltage of $LiVPO_4F$ is ~4.2 V vs. Li, which is 0.2 and 0.7 V higher than that exhibited by $LiCoO_2$ [11] and $LiFePO_4$ [12], respectively; (ii) the phase can be synthesized either by a one-step or a two-step solid-state reaction, at temperatures as low as 550 °C [8], but the optimum appears to be 650–750 °C [1–6,8,9]; (iii) the thermal stability of the charged-cathode is as good as $LiFePO_4$, and much better than $LiCoO_2$ [9]; (iv) demonstration-type Li-ion cells, with mesocarbon micro beads (MCMB) graphite as the counter electrode, have shown very good stability and rate-capability over a large number of cycles [6,7]. In this study, $LiVPO_4F$ is synthesized by a two-step method, characterized, and subjected to long-term cycling (up to 1250 cycles) at 0.12 and 0.92*C* rates at ambient temperature. Complementary cyclic voltammetry and impedance analysis data are reported.

2. Experimental

The compound $LiVPO_4F$ was prepared by mixing stoichiometric amounts of VPO_4 (2.11 g) and LiF (0.387 g) (Merck, 99% purity) using a high energy ball mill (Spex Ball mill (D8000), USA) for 12 h (speed: 1400 rpm, ball:powder ratio (in g): 10:2.5) and heating the mixture at 700 °C for 1 h argon. VPO_4 was prepared by a carbothermal reduction method similar to that used by Barker et al. [1] and involved reacting V_2O_5 (5.42 g, Aldrich; purity, 98%), ammonium dihydrogen phosphate $NH_4H_2PO_4$ (3.93 g, Merck; purity, 99%) and carbon (0.43 g, Super P, surface area: 250 m^2 g^{-1}, 20 wt.% excess carbon). The chemicals were mixed using a mechanical grinder, pelletized and heated at 750 °C for 4 h in flowing argon in a tubular furnace (Carbolite, UK).

X-ray diffraction (XRD) patterns were taken with a Philips Xpert unit with Cu Kα radiation. Lattice parameters were obtained from the XRD data by using TOPAS-R (version 2.1) software and assuming the reported crystal structure. X-ray photoelectron spectra (XPS) of $LiVPO_4F$ were obtained by means of a VG Scientific ESCA MK II spectrometer with monochromatic Mg-K_α radiation (1253.6 eV). The survey spectra were recorded in the range 0–1099 eV with a constant–pass energy of 50 eV. The high-resolution spectra were recorded with a smaller constant pass energy of 20 eV. Charge referencing was carried out against adventitious carbon (C), assuming its binding energy to be 284.6 eV. Analysis of the XPS spectra was done using XPS Peak-fit software. A Shirley-type background was subtracted from the recorded spectra and curve-fitting was conducted with a Gaussian–Lorentzian (ratio, 60:40) curve. The derived binding energies (BE) have accuracy of (±0.2) eV. A scanning electron

* Corresponding author. Tel.: +65 6516 2531; fax: +65 6777 6126.
E-mail address: phychowd@nus.edu.sg (B.V.R. Chowdari).

0378-7753/$ – see front matter © 2010 Elsevier B.V. All rights reserved.
doi:10.1016/j.jpowsour.2010.03.032

microscope (SEM) (JEOL JSM-67500F) and a Micromeritics Tristar 3000, USA and AccuPyc 1330 pycnometer (Micromeritics, USA) were are used to study the morphology, Brunauer, Emmett and Teller (BET) surface area and density, respectively, of the compound.

Composite electrodes were fabricated with the active material, super P carbon and binder (Kynar 2801) in a weight ratio of 70:15:15 by using N-methyl pyrrolidone (NMP) as solvent and an etched aluminum foil (20 μm thickness) as the current-collector. Lithium metal foil (Kyokuto metal Co., Japan) was used as the counter and reference electrode. A solution of 1 M $LiPF_6$ in ethylene carbonate (EC) and dimethyl carbonate (DMC) (1:1, v/v) (Merck) and Celgard 2502 membrane were used as the electrolyte and separator, respectively, to assemble coin-type cells (size, 2016) in an Ar-filled glove-box (MBraun, Germany). The cells were aged for 12 h before measurement. The mass of the active material was varied from 2 to 7 mg and the electrode geometrical area was 2.0 cm^2. Cyclic voltammetry and charge–discharge cycling were carried out at room temperature (RT) by using a computer-controlled Mac-pile II system (Bio-logic, France) and a Bitrode multiple battery tester (Model SCN, Bitrode, USA), respectively. More details of cell fabrication have been described elsewhere [11–13]. For *ex situ* XRD studies of the electrodes, the cells were dismantled in the glove-box and the composite electrodes were recovered, washed with propylene carbonate (anhydrous) solvent, dried and mounted on an oriented Si substrate that acted as the sample holder. Impedance spectra of cells were measured with a Solartron impedance/gain-phase analyzer (model SI 1255) coupled to a potentiostat (SI 1268) at RT (25 °C). The frequency was varied from 0.35 MHz to 3 mHz with an ac signal amplitude of 5 mV. Nyquist plots (Z' vs. $-Z''$) were derived and analyzed using *Z*-plot and *Z*-view software (Version 2.2, Scribner associates Inc., USA).

3. Results and discussion

3.1. Structural aspects

The compound, $LiVPO_4F$ is a crystalline black powder, because it contains some unreacted carbon that is intentionally added during the synthesis of the precursor, VPO_4. The XRD pattern, shown in Fig. 1, indicates that all the peaks can be indexed on the basis of the triclinic structure (space group, $P\bar{1}$) [1–6]. The calculated lattice parameters are: $a = 5.175$ Å, $b = 5.304$ Å, $c = 7.503$ Å, $\alpha = 66.95°$, $\beta = 66.88°$, $\gamma = 81.53°$ and cell volume, 174.06 $Å^3$. These compare well with those reported by Barker et al. [14] ($a = 5.169$ Å, $b = 5.306$ Å, $c = 7.503$ Å, $\alpha = 66.85°$, $\beta = 67.00°$, $\gamma = 81.58°$ and cell volume, 174.21 $Å^3$). Low-intensity lines due to an impurity phase,

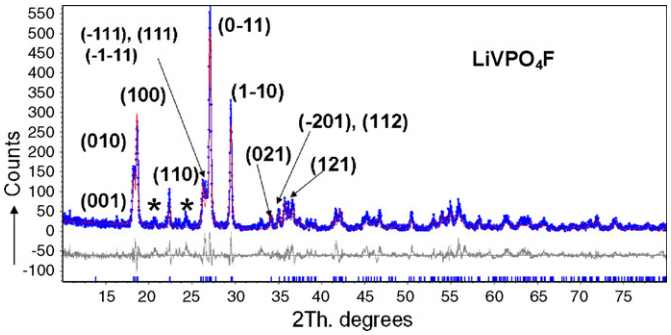

Fig. 1. Powder X-ray diffraction pattern of $LiVPO_4F$. Miller indices are shown. The asterisk denotes impurity, $Li_3V_2(PO_4)_3$. Symbols represent experimental data and continuous line represents fitted pattern. Difference pattern is also shown. Vertical bars represent expected 2θ values. Cu Kα radiation.

namely, $Li_3V_2(PO_4)_3$ [15,16] are also noted in the XRD pattern of Fig. 1. From the relative intensities, it is estimated that the impurity is ≤5 wt. %. The measured density of $LiVPO_4F$ is 3.390 (±0.005) g cm^{-3} and compares well with the calculated value (assuming the formula units per unit cell, $Z = 2$) from the crystal data, namely 3.278 g cm^{-3}. Scanning electron micrographs photographs show agglomeration of sub-micron particles with a plate-like morphology (Fig. 2a and b). The measured BET surface area of $LiVPO_4F$ is 7.7 (±0.2) m^2 g^{-1}, which is typical of well-crystalline oxide materials.

3.2. X-ray photoelectron spectroscopy (XPS)

The core level XPS spectra of $LiVPO_4F$ are shown in the Fig. 3. The binding energy (BE) values of V 2p are 517.1 (±0.2) and 523.4 (±0.2) eV, which correspond to energy level V $2p_{3/2}$ and V$2p_{1/2}$, respectively (Fig. 3a). The splitting of energy levels of V $2p_{3/2}$ and V $2p_{1/2}$ is due to spin orbit coupling, and the energy difference between them is 5.34 eV. The BE value of V $2p_{3/2}$ of $LiVPO_4F$ compares well with the values reported by Li et al. [8] in $LiVPO_4F$ (517.06 eV) and of V 2p in V_2O_3 (517.3 (±0.2) eV) [17] and in $Li_3V_2(PO_4)_3$ (517.7 eV) [18], (517.2 eV) [19] and thereby confirm that the oxidation state of V-ion in $LiVPO_4F$ is 3+. The spectrum of P 2p is shown in Fig. 3b and the BE value of 133.7 (±0.2) eV is characteristic of the tetrahedral PO_4 bond. Similar BE values of P 2p are encountered in $LiFePO_4$ (133.5 eV) [20] and in Li_3PO_4 (133.6 eV) [20] and in $AlPO_4$ (133.4 eV) [21]. The O 1s spectrum has a BE value of 531.2 (±0.2) eV, shown in Fig. 3c, which is due to oxygen predominantly bonded to V or P ions. An additional low-intensity peak with a BE of 533.3 (±0.2) eV may be due to adsorbed water or surface OH-

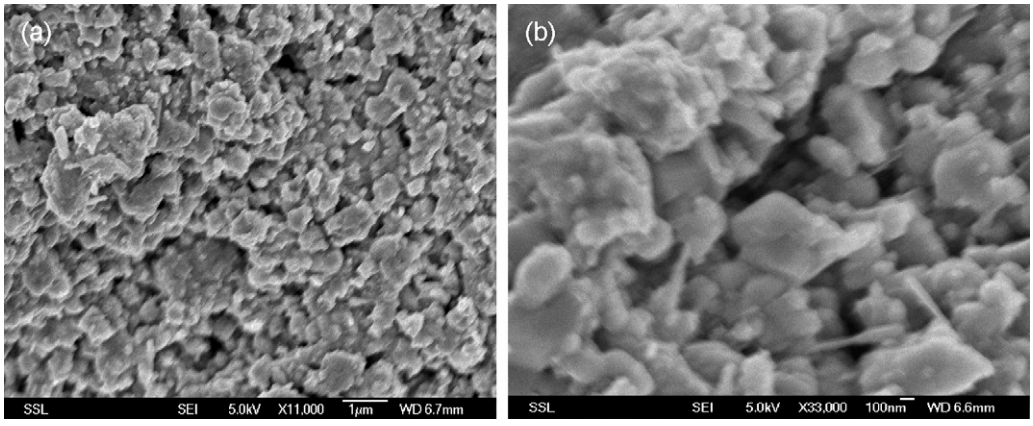

Fig. 2. SEM photographs of $LiVPO_4F$. (a) Bar scale 1 μm; (b) bar scale 100 nm.

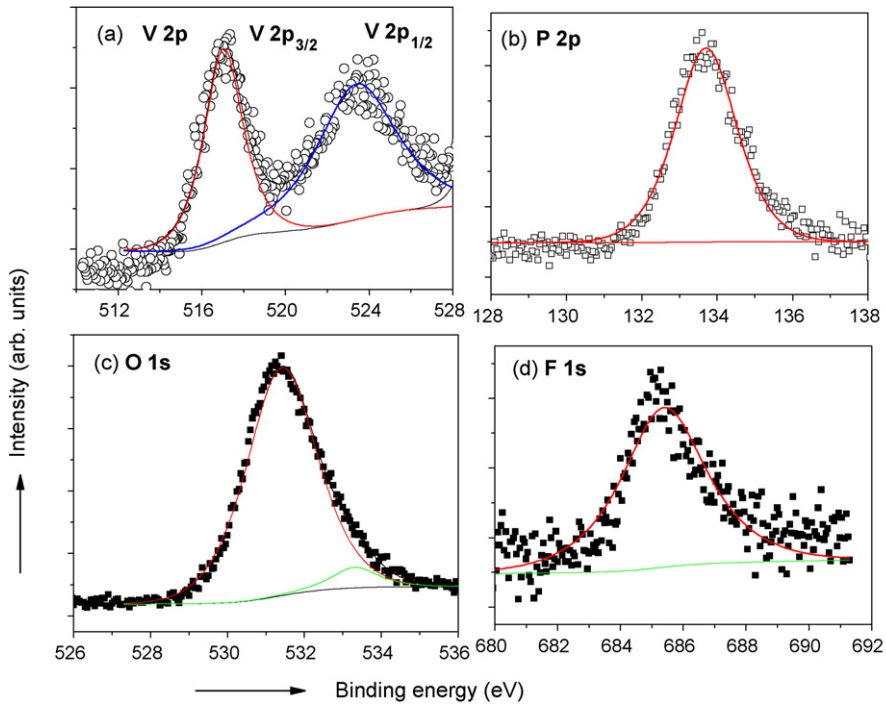

Fig. 3. Core level XPS spectra of $LiVPO_4F$. (a) V 2p, (b) P 2p, (c) O 1s, (d) F 1s. Symbols represent experimental data. Continuous line is fitted data.

groups, similar to the BEs reported for O 1s in $LiFePO_4$ (531.6 and 533.2 eV) [20]. The XPS spectrum of F 1s has a BE value of 685.2 (±0.2) eV, which can be attributed to the V–F bond (Fig. 3d) and this may be compared with the BE of F 1s in LiF, namely, 686.5 eV [22]. It is concluded that the XPS data indeed show the expected valency states of the metal and non-metal ions in $LiVPO_4F$.

4. Electrochemical properties

4.1. Cyclic voltammetry

Cyclic voltammograms (CVs) of $LiVPO_4F$ as a cathode, with Li-metal as the counter and reference electrode, in the potential range 3.0–4.5 V at room temperature and a slow scan rate of 0.058 mV s^{-1} up to 30 cycles are shown in Fig. 4a and b. For clarity, only selected cycles are shown. During the first cycle, three low-intensity anodic peaks (Li-extraction) at 3.60, 3.68 and 4.10 V are noted, followed by a medium intensity peak at 4.25 V and a high intensity, but broad, peak at ~4.45 V. The corresponding main cathodic peak (Li-insertion) is seen at 4.13 V. This is followed by low-intensity cathodic peaks in the potential range 4.05–3.5 V. In the second and subsequent cycles, the medium and high intensity anodic peaks shift to a lower potential (~4.38 V), but the corresponding cathodic peak shifts only by ~0.05 V, to a higher potential. The low-intensity peaks, both anodic and cathodic, in the range 4.1–3.5 V are not shifted. The shift in the peak potentials is an indication of the 'formation' of the electrode in the first few cycles, whereby the active material undergoes minor structural rearrangement and makes good electrical contact with the conducting carbon particles in the composite electrode, the current-collector and the liquid electrolyte. The shifts in the main peak voltages are completed by 5–12 cycles (Fig. 4a). The main anodic and cathodic peak currents show a slight increase up to 25 cycles and thereafter remain constant, as is clear from the CV for the 30th cycle (Fig. 4a and b). The hysteresis (ΔV) of the main anodic and cathodic peak potentials at the 30th cycle is small (0.21 V), which indicates very good reversibility of $LiVPO_4F$. The CV of $LiVPO_4F$ recorded after 1260 galvanostatic cycles shows a slight shift in the main anodic and cathodic peak potentials with $\Delta V = 0.37$ V, indicative of a slight increase in polarization of the electrode. On the other hand, the low-intensity cathodic/anodic peaks in the range 4.05–3.5 V are not shifted (Fig. 4c).

The low-intensity minor anodic peaks at ~3.6–4.10 V and the corresponding cathodic peaks at ~3.56–3.98 V in the CV are almost identical to the peaks observed in the differential capacity vs. voltage curves of $Li_3V_2(PO_4)_3$ [15]. This is convincing proof that the impurity phase in the XRD pattern is indeed $Li_3V_2(PO_4)_3$ (Fig. 1a). The observed CV data on $LiVPO_4F$ are in good agreement with the differential capacity vs. voltage curves (analogous to CV) reported by Barker et al. [4–6] and Li et al. [8] at 4.30 and 4.36 V for Li-extraction, and 4.14 and 4.02 V for Li-insertion, and are assigned to the $V^{3+/4+}$ redox couple.

4.2. Galvanostatic cycling

Galvanostatic cycling of $LiVPO_4F$ as a cathode was carried out at 25 °C up to 300 cycles at a current density of 15 mA g^{-1} and up to 1250 cycles at 120 mA g^{-1} in the voltage range 3.0–4.5 V vs. Li. The voltage vs. capacity profiles of selected cycles at 15 mA g^{-1} are presented in Fig. 5. During the first charge (Li de-intercalation) process, the voltage increases to ~4.0 V from the open-circuit voltage (OCV ~3.0 V) with a small plateau at ~4.1 V till about 10 mAh g^{-1} of capacity is reached, followed by a wide plateau region at 4.28 V, till a charge capacity of about 130 (±3) mAh g^{-1}. The total first charge capacity is 140 (±3) mAh g^{-1} vs. the theoretical value, 156 mAh g^{-1} (Fig. 5a). The first discharge profile shows a voltage plateau at ~4.2 V with minor steps in the low-voltage region, and the total capacity is 123 (±3) mAh g^{-1}. Thus, the irreversible capacity loss during the first cycle is 17 (±3) mAh g^{-1} which corresponds to a coulombic efficiency of 88%. During subsequent charge and discharge cycles, the plateau voltage values remain almost the same. The discharge capacity shows an increasing trend up to about 10–15 cycles and thereafter becomes almost the same as the charge capacity, which

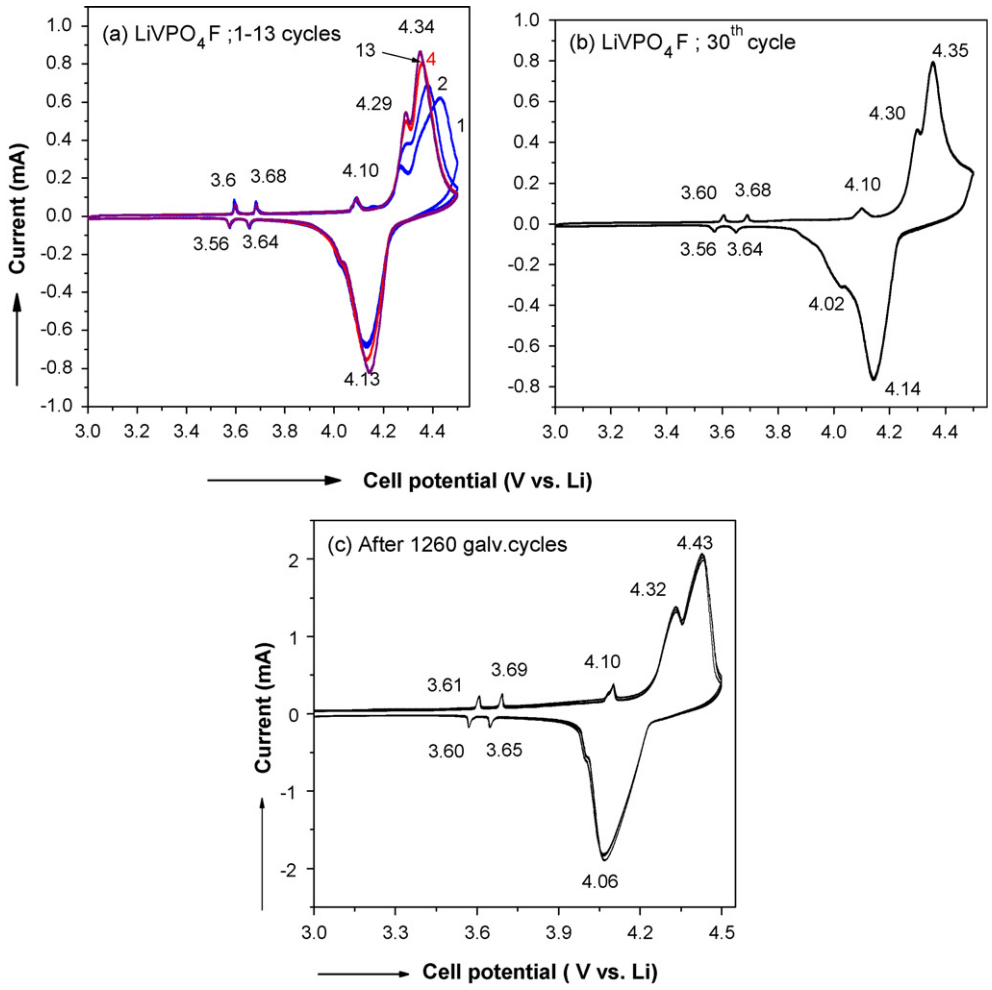

Fig. 4. Cyclic voltammograms of $LiVPO_4F$ in potential range 3.0–4.5 V vs. Li. Scan rate, 58 $\mu V\,s^{-1}$. (a) 1–13 cycles; only selected cycles (1, 2, 4, 13) shown. (b) 30th cycle. (c) After 1260 galvanostatic cycles at 0.92*C* rate. Numbers indicate potentials in volts. *y*-Axis values are higher in comparison with (a) and (b) due to larger active mass of material (5.81 mg vs. 1.82 mg).

indicates an increase in the coulombic efficiency to 96–98%. The capacity vs. cycle number plot in Fig. 5d shows a stable capacity of 130 (±3) mAh g^{-1} over 40–150 cycles. A slow capacity degradation is observed in the range 150–360 cycles, at the rate of 0.02 mAh g^{-1} per cycle. Also the ΔV, the difference between the average charge and discharge voltage, slightly increases from 0.11 V at the 100th cycle to 0.23 V at the end of 360th cycle, indicating an increase in the electrode polarization (Fig. 5b and c). The differential capacity vs. voltage plot, derived from the voltage-capacity profile of the 360th cycle (Fig. 5b), is shown in Fig. 5c and bears a very good resemblance to the CV curves of Fig. 4b and c.

Galvanostatic cycling data in the form of voltage vs. capacity profiles of $LiVPO_4F$ at 120 mA g^{-1} (0.92*C*, assuming 1*C* = 130 mA g^{-1}) in the voltage range 3.0–4.5 V are given in Fig. 6a. The plateau voltage values are the same as those encountered when cycled at 15 mA g^{-1} (0.12*C* rate). As can be expected, the first charge and discharge capacities are 109 and 106 (±3) mAh g^{-1}, respectively, which are smaller than the values measured at the 0.12*C* rate. With increase in cycle number, there is an increase in the reversible capacity due to the 'formation' (formatting) of the electrode, which stabilizes at 122 (±3) mAh g^{-1} at the end of 200 cycles. This capacity remains more or less stable up to 800 cycles, after which it slowly degrades to 105 (±3) mAh g^{-1} at the end of the 1250th cycle (Fig. 6b), and corresponds to a capacity-fade of 14% in the range 800–1250 cycles. The capacity fading observed at the 0.12*C* rate after 150 cycles, and at 0.92*C* rate after 800 cycles, could be due to slight polarization of the electrode because of the two-phase reaction, and to drying-up of the electrolyte as a result of long-term cycling. The observed capacity values are in good agreement with those reported by Barker et al. [1–7] and others [8–10].

The *ex situ* XRD patterns of $LiVPO_4F$ cycled electrodes in the discharged state (at 3.0 V) after 40 cycles, and in the charged state (at 4.5 V) after 90 cycles are shown in Fig. 7, along with that of the bare electrode $LiVPO_4F$. The patterns overlap well, except for slight changes in the relative intensities of selected peaks and no new peaks are seen. This indicates that the parent structure, as well as the Li-vacant structure, is completely analogous due to the fact that Li-cycling proceeds through a two-phase reaction, namely, $LiV^{3+}PO_4F \leftrightarrow \square V^{4+}PO_4F + Li^+ + e^-$, where e^- is the electron and □ is the vacancy. Of course, slight changes in the crystal lattice parameters and angles occur in $\square V^{4+}PO_4F$, as compared with the parent phase ($LiV^{3+}PO_4F$) due to the smaller ionic radius of the V^{4+} ion and relaxation of the crystal lattice as a result of the vacancy at the Li-site. Similar structural similarities between the parent and product phases during the charge–discharge process have also been established in cathode materials such as, $LiFePO_4$ [23] and $Li_3V_2P_3O_{12}$ [15], and the anode material $Li_4Ti_5O_{12}$ [24].

4.3. Impedance spectroscopy studies

Electrochemical impedance spectroscopy (EIS) is a useful technique for studying the electrode kinetics of LIB cathode materials

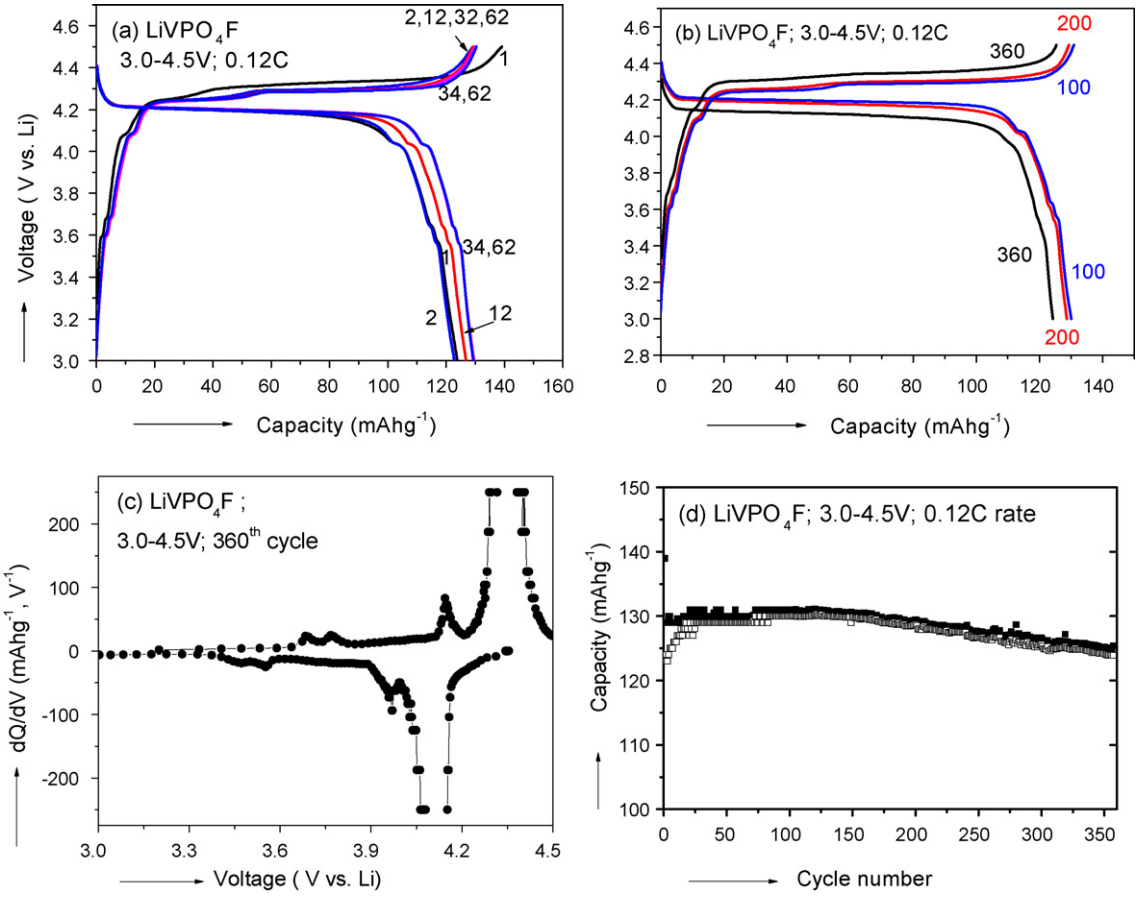

Fig. 5. Galvanostatic cycling profiles of $LiVPO_4F$. Voltage range 3.0–4.5 V vs. Li at current rate 15 mA g^{-1} (0.12*C*); only selected cycles shown for clarity: (a) 1–62 cycles; (b) 100–360 cycles; numbers indicate cycle number. (c) Differential capacity (dQ/dV) vs. voltage (V) plot for 360th cycle, extracted from (b). (d) Capacity vs. cycle number plot. Voltage range 3.0–4.5 V, current rate 15 mA g^{-1} (0.12*C*). Filled symbols: charge capacity; open symbols: discharge capacity.

in which Li-cycling occurs in single-phase [25–27] and two-phase reactions [28–34]. Nevertheless, EIS studies on $LiVPO_4F$ have not been reported in the literature. In the present investigation, the impedance spectra are measured with Li-metal as the counter electrode at various voltages (3.0–4.5 V) at the 0.12*C* rate during the first cycle, and also in the discharged or charged state after a given number of cycles in the range of 30–90 cycles. The Nyquist plots (Z' vs. $-Z''$) are shown in Fig. 8 where Z' and Z'' represent the real and imaginary part of the impedance. The spectra were fitted to an equivalent circuit consisting of resistances (both electrolyte and charge-transfer), a constant phase element (CPE) in lieu of the capacitance (C_i), a Warburg impedance and an intercalation capacitance [26–34]. The α values were calculated using the equation, $Z_{CPE} = 1/[\beta(j\omega)^{\alpha}]$ where Z_{CPE} is the impedance of CPE_i, ω is the angular frequency, $j = \sqrt{-1}$ and β and α are constants. The value of α indicates the degree of dis-

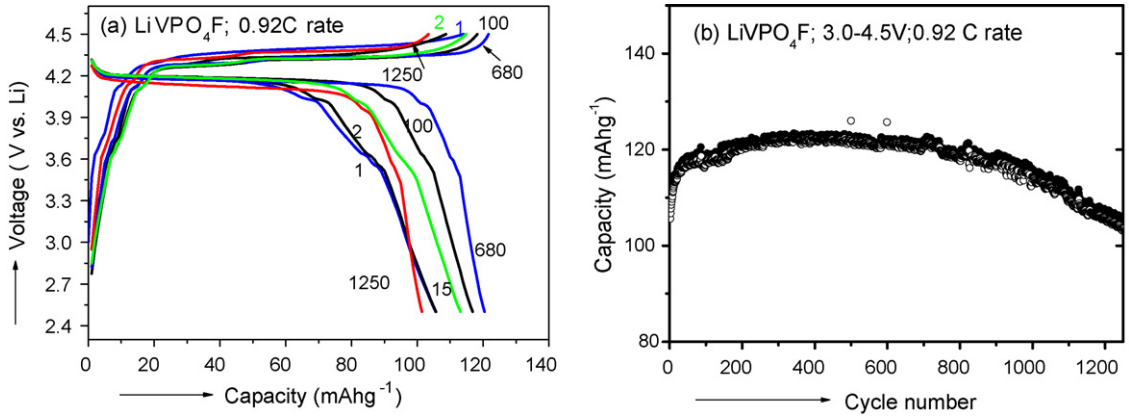

Fig. 6. (a) Galvanostatic cycling profiles of $LiVPO_4F$ in voltage range 3.0–4.5 V at current of 120 mA g^{-1} (0.92*C*, assuming 1*C* = 130 mA g^{-1}) up to 1250 cycles. Numbers indicate cycle number. Only selected cycles (1, 2, 15, 100, 680, 1250) shown for clarity. (b) Capacity vs. cycle number plot derived from data of (a). Filled symbols: charge capacity; open symbols: discharge capacity.

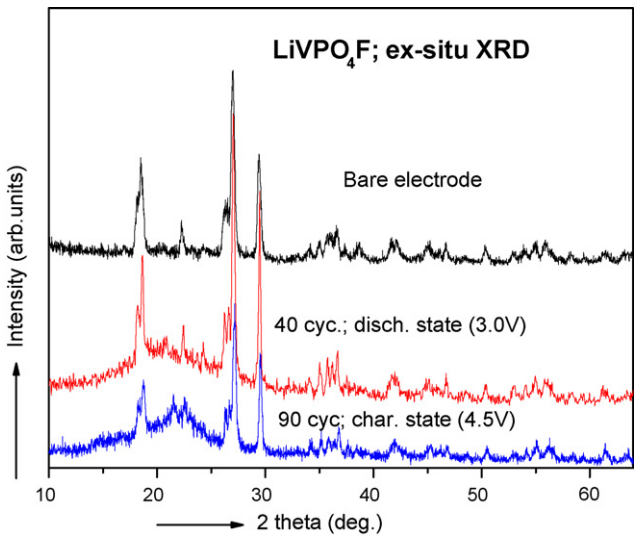

Fig. 7. Ex situ XRD patterns of composite $LiVPO_4F$ electrode and cycled electrodes in discharged state (3.0 V) after 40 cycles, and in charged state (4.5 V) after 90 cycles. Relative intensities (y-axis) are normalized for better comparison. Cu Kα radiation.

tortion of the impedance spectra from ideal behaviour; when $\alpha = 1$, β is identical to C_i and CPE_i becomes an ideal capacitor.

A fresh cell (OCV~3 V) shows a single semicircle in the frequency range 0.18 MHz to 17 Hz, followed by a Warburg region (Fig. 8a). The fitted values of surface-film resistance (R_{sf}) and surface-film capacitance (CPE_{sf}) are 37 (±3) Ω and 24 (±3) μF, respectively (Table 1). During both the charge- and -discharge cycles a single semicircle is observed and therefore the spectra are fitted using a combination of surface-film and charge-transfer resistance ($R_{(sf+ct)}$) and the corresponding $CPE_{(sf+dl)}$, where dl refers to double layer capacitance. The R_{ct} arises due to the resistance at the interface between the electrode and electrolyte. The $R_{(sf+ct)}$ values during the first charge cycle increase from 40 to 164 (±3) Ω in the voltage range 3.6–4.5 V whereas the corresponding $CPE_{(sf+dl)}$ values remain constant at 26 (±5) μF (Table 1). The fourfold increase in $R_{(sf+ct)}$ when the voltage is increased from 3.6 to 4.5 V is understandable since the Li-deintercalated phase ($\square VPO_4F$) will have a higher resistance than the pristine phase. The α-values range from 0.79 to 0.82. During the first discharge cycle, in the voltage range 4.0–3.0 V, $R_{(sf+ct)}$ varies from 158 to 86 (±3) Ω and $CPE_{(sf+dl)}$ values range from 34 to 46 (±5) μF. Thus, the resistance values during the charge cycle show an increasing trend from 3.0 to 4.5 V and a decreasing trend during the discharge cycle to 3.0 V. The $R_{(sf+ct)}$ at 3.0 V at the end of first cycle is 86 (±3)Ω, a twofold increase when compared with the original starting-value. The α-values are in the range 0.72–0.76, i.e., smaller than those encountered during the charge cycle.

As can be seen in Fig. 8c and d, both in the charged state and in the discharged state only a single semicircle is noted, similar to the first-cycle spectra. In the range 30–50 cycles, the spectra almost overlap, which indicates that the impedance parameters remain more or less constant. Thus, $R_{(sf+ct)}$ values range from 60 to 71 (±3) Ω in the charged state (4.5 V), and from 97 to 110 (±3) Ω in the discharged state (3.0 V). At the end of 60, 70 and 90 cycles, however, these values show an increasing trend with an increase in the cycle number, as are the α values (Table 1). The $CPE_{(sf+dl)}$ values, on the other hand, show a decreasing trend with increasing cycle number, both in the charged state and in the discharged state. The observed trends in the impedance parameters indicate an increase in the polarization of the $LiVPO_4F$ electrode that is also evident in CV and galvanostatic cycling data.

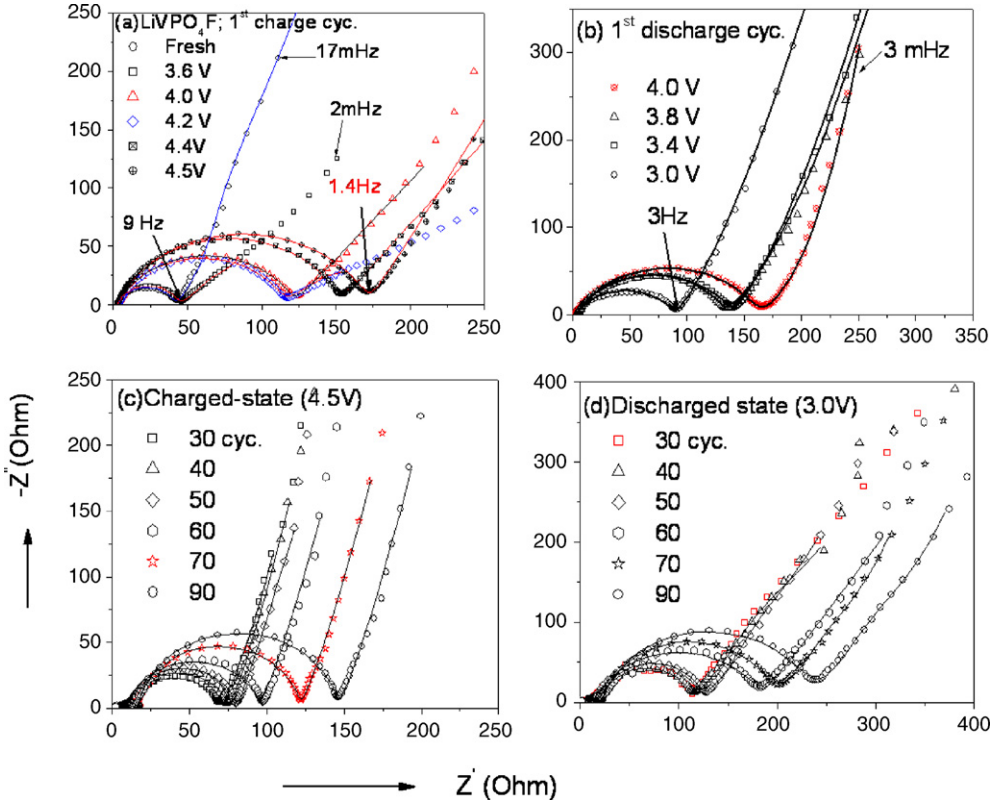

Fig. 8. Nyquist plots (Z' vs. $-Z''$) of cell, $LiVPO_4F$ vs. Li during (a) first charge cycle and (b) first discharge cycle; selected frequencies are shown. Nyquist plots at various cycle numbers: (c) in charged state (4.5 V) and (d) discharged state (3.0 V). Symbols represent experimental data and continuous lines represent fitted spectra using equivalent circuit. Geometrical area of electrode is 2 cm^2.

Table 1
Impedance parameters of system, $LiVPO_4F$-Li during first charge–discharge cycle at various voltages, and as a function of cycle number in fully charged state and discharged state.

Parameter						
First charge cycle						
Cell voltage, V vs. Li	3.0 (OCV)	3.6	4.0	4.2	4.4	4.5
$R_{(sf+ct)}$ (±3) Ω	38	40	112	110	148	164
$CPE_{(sf+dl)}$ (±3) μF	24	27	26	29	30	31
α (±0.02)	0.82	0.82	0.80	0.79	0.82	0.81
First discharge cycle						
Cell voltage, V vs. Li	3.0	3.4	3.8	4.0		
$R_{(sf+ct)}$ (±3) Ω	86	131	136	158		
$CPE_{(sf+dl)}$ (±3) μF	46	38	34	34		
α (±0.02)	0.72	0.74	0.76	0.74		
Cycle number: discharged state Cell voltage, 3.0 V vs. Li	30	40	50	60	70	90
$R_{(sf+ct)}$ (±3) Ω	97	100	110	164	169	202
$CPE_{(sf+dl)}$ (±3) μF	72	73	67	77	58	60
α (±0.02)	0.83	0.83	0.87	0.81	0.89	0.88
Cycle number: charged state Cell voltage, 4.5 V vs. Li	30	40	50	60	70	90
$R_{(sf+ct)}$ (±3) Ω	60	67	71	84	104	127
$CPE_{(sf+dl)}$ (±3) μF	77	71	61	64	51	54
α (±0.02)	0.83	0.84	0.89	0.88	0.93	0.92

5. Conclusions

The compound, $LiVPO_4F$ with a triclinic structure has been prepared by a two-step carbothermal reduction method and then characterized by X-ray diffraction, X-ray photoelectron spectroscopy, SEM, surface area and density techniques. A minor impurity phase, $Li_3V_2P_3O_{12}$, is noted in the synthesized material. Electrochemical studies have been carried out by cyclic voltammetry (CV) and galvanostatic cycling, at room temperature. Charge–discharge cycling of $LiVPO_4F$ in the voltage range 3.0–4.5 V at a current rate of 15 mA g^{-1} (0.12 C) shows a reversible capacity of 130 (±3) mAh g^{-1} in the range of 20–200 cycles and then a slow capacity fading between 200 and 360 cycles. When cycled at the 0.92*C* rate (1*C* = 130 mA g^{-1}), a reversible capacity of 122 (±3) mAh g^{-1} is observed and is stable between 200 and 800 cycles. The capacity degrades slowly over 800–1260 cycles, with a capacity loss of 14%. The coulombic efficiency increases to 96–98% after the first 10–15 cycles. CV data show a clear indication of the $V^{3+/4+}$ redox couple at ~4.35–4.15 V that involves a two-phase reaction. Impedance spectra are measured during the first cycle and as a function of cycle number (up to 90 cycles) in the fully charged state and the discharged state. The spectra have been fitted to an equivalent circuit and the variation of impedance parameters interpreted. The observed cycling behaviour and CV data corroborate the studies up to 200 cycles reported in the literature, and indicate that $LiVPO_4F$ can function to at least 800 cycles at the 0.92*C* rate with good reversible capacity. It is therefore a viable 4 V-cathode for LiBs.

References

[1] J. Barker, M.Y. Saidi, J.L. Swoyer, J. Electrochem. Soc. 150 (2003) A1394.
[2] J. Barker, M.Y. Saidi, J.L. Swoyer, J. Electrochem. Soc. 151 (2004) A1670.
[3] J. Barker, R.K.B. Gover, P. Burns, A. Bryan, Electrochem. Solid State Lett. 8 (2005) A285.
[4] J. Barker, R.K.B. Gover, P. Burns, A. Bryan, M.Y. Saidi, J.L. Swoyer, J. Electrochem. Soc. 152 (2005) A1776.
[5] J. Barker, R.K.B. Gover, P. Burns, A. Bryan, Electrochem. Solid Lett. 8 (2005) A130.
[6] H. Huang, T. Faulkner, J. Barker, M.Y. Saidi, J. Power Sources 189 (2009) 748.
[7] R.K.B. Gover, A. Bryan, P. Burns, J. Barker, Solid State Ionics 177 (2006) 1495.
[8] Y.Z. Li, Z. Zhou, X.P. Gao, J. Yan, J. Power Sources 160 (2006) 633.
[9] F. Zhou, X.M. Zhao, J.R. Dahn, Electrochem. Commun. 11 (2009) 589.
[10] S.K. Zhong, J. Wang, Y.W. Li, L.T. Liu, J.Q. Liu, J.W. Yang, Chem. Lett. 38 (2009) 374.
[11] K.S. Tan, M.V. Reddy, G.V. Subba Rao, B.V.R. Chowdari, J. Power Sources 147 (2005) 241.
[12] K. Saravanan, M.V. Reddy, P. Balaya, H. Gong, B.V.R. Chowdari, J.J. Vittal, J. Mater. Chem. 19 (2009) 605.
[13] M.V. Reddy, G.V. SubbaRao, B.V.R. Chowdari, J. Power Sources 160 (2006) 1369.
[14] J. Barker, R.K.B. Gover, P. Burns, A. Bryan, M.Y. Saidi, J.L. Swoyer, J. Power Sources 146 (2005) 516.
[15] M.Y. Saidi, J. Barker, H. Huang, J.L. Swoyer, G. Adamson, Electrochem. Solid State Lett. 5 (2002) A149.
[16] X.J. Zhu, Y.X. Liu, L.M. Geng, L.B. Chen, H.X. Liu, M.H. Cao, Solid State Ionics 179 (2007) 1679.
[17] J. Mendialdua, R. Casanova, Y. Barboux, J. Electron Spectrosc. Relat. Phenom. 71 (1995) 249.
[18] Q. Chen, J. Wang, Z. Tang, W. He, H. Shao, J. Zhang, Electrochim. Acta 52 (2007) 5251.
[19] M. Ren, Z. Zhou, Y. Li, X.P. Gao, J. Yan, J. Power Sources 162 (2006) 1357.
[20] Y.-H. Rho, L.F. Nazar, L. Perry, D. Ryan, J. Electrochem. Soc. 154 (2007) A283.
[21] K.S. Tan, M.V. Reddy, G.V. Subba Rao, B.V.R. Chowdari, J. Power Sources 141 (2005) 129.
[22] H. Bryngelsson, M. Stjerndahl, T. Gustafsson, K. Edstrom, J. Power Sources 174 (2007) 970.
[23] A. Yamada, H. Koizumi, S.-I. Nishimura, N. Sonoyama, R. Kanno, M. Yonemura, T. Nakamura, Y. Kobayashi, Nat. Mater. 5 (2006) 357.
[24] K. Ariyoshi, R. Yamato, T. Ohzuku, Electrochim. Acta 51 (2005) 1125.
[25] K.M. Shaju, G.V. Subba Rao, B.V.R. Chowdari, J. Electrochem. Soc. 151 (2004) A1324.
[26] F. Nobili, S. Dsoke, F. Croce, R. Marassi, Electrochim. Acta 50 (2005) 2307.
[27] M.V. Reddy, G.V. Subba Rao, B.V.R. Chowdari, J. Phys. Chem. C 111 (2007) 11712.
[28] H. Joachin, T.D. Kaun, K. Zaghib, J. Prakash, J. Electrochem. Soc. 156 (2009) A401.
[29] G.X. Wang, D.H. Bradhurst, S.X. Dou, H.K. Liu, J. Power Sources 83 (1999) 156.
[30] H.C. Shin, W.I. Cho, H. Jang, J. Power Sources 159 (2006) 1383.
[31] M. Koltypin, D. Aurbach, L. Nazar, B. Ellis, Electrochem. Solid-State Lett. 10 (2007) A40.
[32] S.-C. Yin, P.S. Strobel, H. Grondey, L.F. Nazar, Chem. Mater. 16 (2004) 1456.
[33] Y. Li, X. Liu, J. Yan, Electrochim. Acta 53 (2007) 474.
[34] A. Tang, X. Wang, G. Xu, Z. Zhou, H. Nie, Mater. Lett. 63 (2009) 1439.